RESEARCH ARTICLE
doi: 10.2306/scienceasia1513-1874.2025.039

ScienceAsia 51 (3): 2025: ID 2025039: **1–11**

Cellular antioxidative and regenerative potentials of *Clinacanthus nutans* leaf fractions towards liver cells: An integrated *in vitro* and *in silico* study

Kai Song Ng[a], Siew Lee Cheong[b], Vick Key Tew[c], Li Ting Kee[c], Jia Xian Law[c], Khye Er Loh[a], Chen Son Yue[d], Chui Fung Loke[a], Sheri-Ann Tan[a,*]

[a] Department of Bioscience, Faculty of Applied Sciences, Tunku Abdul Rahman University of Management and Technology, Kuala Lumpur 53300 Malaysia
[b] Department of Pharmaceutical Chemistry, School of Pharmacy, International Medical University, Kuala Lumpur 57000 Malaysia
[c] Department of Tissue Engineering and Regenerative Medicine, Faculty of Medicine, Universiti Kebangsaan Malaysia, Kuala Lumpur 56000 Malaysia
[d] Department of Physical Science, Faculty of Applied Sciences, Tunku Abdul Rahman University of Management and Technology, Kuala Lumpur 53300 Malaysia

*Corresponding author, e-mail: tansw@tarc.edu.my

Received 16 Mar 2024, Accepted 11 Mar 2025
Available online 28 May 2025

ABSTRACT: *Clinacanthus nutans* (Burm.f.) Lindau is a medicinal plant used for treatment of liver cancer and jaundice by Chinese healers. This study aimed to determine the phytocompounds that contribute to the antioxidative and regenerative potentials of *C. nutans* leaves when examined on the HepG2 liver cells and the umbilical cord-derived mesenchymal stem cells, respectively. NMR-based metabolomics approach and molecular docking were employed to identify contributing phytocompounds. All fractions were found non-toxic towards both cell lines when tested at concentration up to 100 µg/ml. It was shown that cells treated with hexane and ethyl acetate fractions were able to reduce ROS levels by 36% and 27.6% respectively, during oxidative stress when measured at 120 min as compared to untreated cells. Furthermore, hexane fraction increased glutathione levels in HepG2 cells by approximately 3-fold whereas ethyl acetate fraction treated cells showed 2.36-fold increment of glutathione in comparison to untreated control. Hexane fraction demonstrated slight regenerative potential towards mesenchymal stem cells. Ethyl acetate fraction, on the contrary, retarded this activity. Interestingly, phytocompounds: clinacoside B, clinacoside C and isoschaftoside which were postulated earlier to play important roles in *C. nutans* leaves antioxidative properties were detected in hexane fraction through NMR analysis. Amongst them, isoschaftoside formed interactions with important amino acid residues within the binding pocket of Keap1 *in silico* suggesting its strong inhibitory effect towards this protein. Isoschaftoside is thus a promising compound to be further investigated as a treatment for chronic liver problems such as non-alcoholic fatty liver disease.

KEYWORDS: *Clinacanthus nutans*, antioxidant, liver regeneration, isoschaftoside, Nrf2

INTRODUCTION

The primary contributor to chronic liver disease is non-alcoholic fatty liver disease (NAFLD) [1]. NAFLD, a severe clinicopathological condition, is widely regarded as the most prevalent chronic liver disorder, impacting between 14% to 30% of the global population. There has been a spike in cases of NAFLD, which is commonly associated with the rise in obesity and also type 2 diabetes [2]. This liver disease can cause serious long-term complications such as liver cirrhosis, liver fibrosis, and cardiovascular disorders [3]. In fact, NAFLD development and the disease progression involves multiple mechanisms leading to oxidative stress which plays important roles in the pathophysiology of this disease [4].

The concept of oxidative stress implies that there is an unequal balance between the ability of antioxidants to counteract reactive oxygen species (ROS) and other oxidants, resulting in an excess of these radicals, which have detrimental effects on cellular functions. When the action of antioxidants is compromised or limited, it will lead to accumulation of ROS, ultimately contributing to the development of various diseases such as fatty liver disease [5]. ROS are produced as a result of aerobic metabolism and primarily consist of the superoxide anion, hydroxyl radicals, and hydrogen peroxide. These molecules have the ability to react with a variety of targets and are involved in a wide range of physiological and pathological processes [6]. Due to the unique characteristics of ROS, it can initiate oxidation alterations to macromolecules, which results in liver injury [7]. This contributes to stellate cell activation, chronic inflammatory response and development of hepatic fibrosis [8].

In the past decades, various therapeutics were prescribed for treating NAFLD such as hypoglycemic drugs, farnesoid X activated receptor (FXR) agonists, statins, and antioxidants [9]. Clinical evidences have proven that dietary supplement with a variety of

polyphenols significantly enhances prognosis of individuals with NAFLD. Moreover, multiple signaling pathways are reported to be involved in the remedial effects of antioxidants in NAFLD in which the activation of Nrf2 pathway has been the most investigated [10]. Nrf2 activators from natural or synthetic sources have been utilized as potential therapies for this disorder [4]. In view of that, antioxidative phytochemicals from *Clinacanthus nutans* (Burm.f.) Lindau may possess the potential to prevent the progression of NAFLD through Nrf2 activation.

C. nutans is a perennial herbal plant from the Acanthaceae family. It is also known by its common names such as "belalai gajah" (Malay), "phaya yo" (Thai), Sabah snake grass, "ki tajam" (Sunda), "dandang gendis" (Jawa), and "e zui hua" or "you dun cao" (Mandarin). This plant is mainly found in China, Thailand, Malaysia, and Indonesia. It possesses drooping branches that can grow up to three metres tall [11]. *C. nutans* is used traditionally for treating various diseases including liver cancer and jaundice by Chinese healers [12]. The leaves extract was scientifically proven to exhibit a range of pharmacological properties which includes antioxidative, anti-inflammatory and analgesic effects [13]. It contains phytochemicals such as flavonoids, sulphur-containing compounds (2-*cis*-entadamine A, entadamine A and C), sulphur-containing glycosides (clinacoside A, B, C, cycloclinacoside A1 and A2), terpenes, phytosterols, and phenolic compounds [12, 14], common to medicinal plants.

Our preliminary work demonstrated that the methanolic leaves extract of *C. nutans* was non-toxic to the liver cells at the concentration range tested but instead showed pro-proliferative effects which indicated healthier cellular growth. In addition, the extract exerted good antioxidative activities in cell-based assays. Based on multivariate analysis of NMR-based metabolomic data of the samples, the phytocompounds postulated to be responsible for *C. nutans* leaves bioactivities were clinacoside B, clinacoside C, and isoschaftoside [15]. Therefore, we are interested to further investigate the liver protective potential of the different fractions of the leaves extract of *C. nutans*. In addition, the secondary metabolites that hold responsible for both antioxidative and regenerative potentials would be identified.

MATERIALS AND METHODS

General materials

Analytical (AR) grade ethyl acetate, n-hexane and n-butanol were purchased from Merck (USA). Hybrimax dimethylsulfoxide (DMSO), cell grade 3-(4,5-dimethylthiazole-2-yl)-2,5-diphenyl tetrazolium bromide (MTT) powder, dichloro-dihydro-fluorescein diacetate (DCFH-DA) were obtained from Sigma-Aldrich (USA). Alpha-Minimum Essential Medium (α-MEM) was procured from Nacalai Tesque (Japan) while Dulbecco's Modified Eagle Medium (DMEM), trypsin-EDTA, fetal bovine serum (FBS) and the antibiotic, penicillin-streptomycin were products of Gibco (USA).

Cell culture

HepG2, a human liver cancer cell line, was obtained from the American Type Culture Collection (ATCC). HepG2 cells were cultured in α-MEM containing 10% FBS and 1% pen-strep. Human Wharton's jelly-derived mesenchymal stem cells (WJ-MSCs), on the other hand, were obtained from the primary cell bank of the Department of Tissue Engineering and Regenerative Medicine (DTERM) at the National University of Malaysia. The cells were cultured in DMEM supplemented with 10% human platelet lysate and 1% antibiotic-antimycotic. Both cells were grown in humidified atmosphere with 5% CO_2 at 37 °C.

Extraction of *C. nutans* leaves extracts

C. nutans leaves were purchased in April 2018 from a farm located in Jelebu (Negeri Sembilan) known as TKC Herbal Nursery Sdn Bhd. Authentication of the plant specimen was performed at the herbarium of the Biodiversity Unit, University Putra Malaysia (UPM), Serdang, Malaysia. The voucher number allocated for our sample was SK3266/17. Oven-dried leaves were first ground into fine powder. Maceration of powdered samples in 80% methanol was carried out based on previous work [15]. Extracts were concentrated at 40 °C by using a rotary evaporator (R-100 series, Buchi, Switzerland). After that, the sample was placed in a −80 °C freezer overnight. The frozen sample was subjected to freeze drying (CoolSafe-9L, ScanVac, Denmark). The freeze-dried powdered extracts were stored in −20 °C freezer for future experiments.

Fractionation of crude *C. nutans* leaves extracts

C. nutans leaves extracts were fractionated by liquid-liquid partition chromatography using hexane, ethyl acetate, n-butanol, and water. About 10 g of crude *C. nutans* leaves extracts were dissolved in 100 ml distilled water and sonicated for 30 min at 50 °C. The mixture was transferred into a separating funnel with 250 ml capacity and fractionated using 100 ml of hexane. After shaken vigorously, the mixture was set aside until two layers were formed. The water layer produced was removed. This process was repeated 4 times. The water residue obtained was then fractionated by repeating the procedures above, while replacing hexane with other solvents (n-butanol and ethyl acetate). The residual solvent was removed from the extracted fractions by drying in oven at 60 °C. After that, the extracted fractions were frozen under −80 °C for 24 h before subjected to freeze drying for 72 h and stored at −20 °C freezer until use [16].

Cell-based antioxidative assays

Cytotoxicity assay

The HepG2 cells were seeded (1×10^4 cells/well in 96-well plates) and cultured for 48 h. After incubation, the cells were washed using 1X PBS before being treated with fractions of *C. nutans* leaves extracts at concentrations ranging from 5 to 100 µg/ml. After 24 h at 37 °C in a 5% CO_2 incubator, the cells were washed with 1X PBS twice, followed by the addition of 100 µl of fresh media into each well. After that, 10 µl of MTT solution (5 mg/ml) was added and incubated for 2.5 h. Finally, 100 µl of 10% SDS was pipetted into each well and left for another 18 h. The colour change was quantified using microplate reader at 540 nm absorbance [17].

Innate ROS level without oxidative stress

First, HepG2 cells were seeded in a 24-well microplate at a concentration of 2×10^5 cells per well. When cells reached a confluency of 70%, they were treated with three different concentrations (6.25, 12.5 and 25 µg/ml) of fractions. After 20 h, 5 µM DCFH was added to the wells for 30 min at 37 °C before washing the cells twice with 1X PBS. Then, 0.5 ml of serum-free medium was added per well. The 24-well plate was immediately measured (time 0) in a fluorescent microplate reader at an excitation wavelength of 485 nm and an emission wavelength of 530 nm. The plate was measured every 30 min for 1 h [16].

Cellular ROS level after induced-oxidative stress

HepG2 cells were first plated in a 24-well microplate at a density of 2×10^5 cells per well prior to treatment with three concentrations (6.25, 12.5 and 25 µg/ml) of leaves fractions. After 20 h, 5 µM DCFH was pipetted into the wells and incubated for 30 min at 37 °C. Then, 400 µM of tert-butyl hydroperoxide (t-BOOH) was added and the cells were incubated for 20 min. Then, cells were washed with 1X PBS prior to the addition of 0.5 ml of serum-free α-MEM medium. The 24-well plate was immediately measured using similar protocol as mentioned for the Innate ROS. The plate was monitored at 60 min and 120 min [16].

Glutathione (GSH) assay

Total glutathione was assessed using Oxiselect™ Total Glutathione (GSSG/GSH) Assay Kit (Cell Biolabs, INC, USA). Briefly, HepG2 cells were cultured at 1.5×10^4 cells/well in 24-wells cell culture plates for 24 h. After that, the culture medium was replaced with FBS-free medium containing 25 µg/ml concentrations of *C. nutans* fractions and incubated for another 24 h. Then the cells were harvested and lysed using an ultrasonic bath. The lysates were centrifuged and the supernatant was used for the determination of protein content using Bradford assay. Briefly, 1 ml of Bradford reagent was mixed with 5 µl of sample in a cuvette. Absorbance was read through a spectrophotometer at 595 nm with reference to the bovine serum albumin (BSA) standard curve. The GSH levels, on the other hand, was determined based on the product manufacturer's specifications [18].

WJ-MSC culture

WJ-MSCs cytotoxicity assay

A total of 1×10^4 WJ-MSCs were seeded in 96-well plates for 24 h before treated with the hexane and ethyl acetate fractions at concentration 0, 5, 10, 20, 40, 80 and 100 µg/ml for 24 h. Then, 10 µl of CCK8 (Elabscience, China) were added. The cells were incubated for 2 h before the absorbance was read with a microplate reader at 450 nm.

WJ-MSCs cell proliferation assay

A total of 1.9×10^4 WJ-MSCs were seeded in 12-well plates in the presence of 0, 10, 25 and 50 µg/ml of hexane and ethyl acetate fractions. The medium was changed every 2 days and the cell count was performed using the trypan blue exclusion assay to determine the cell viability and total cell number once the culture reached 90% confluence. The population doubling time (PDT) was calculated using the following formula:

$$\text{PDT} = \frac{t \log 2}{\log N_2 - \log N_1},$$

where t = time in culture (h), N_2 = cell number at the of culture, and N_1 = cell number seeded.

WJ-MSCs migration assay

A total of 1.9×10^4 WJ-MSCs were seeded in 12-well plates. Upon reaching 70–80% confluence, the cells were starved with serum-free medium overnight prior to the treatment. A scratch was made on the cell monolayer with a sterile 10 µl pipette tip. Subsequently, 0, 10, 25 and 50 µg/ml of hexane and ethyl acetate fractions were added into each well. Scratch closure was monitored at 0, 12 and 24 h using an inverted microscope (Nikon, Japan). Scratch areas were measured by Image-J Software (NIH, USA). Wound closure was calculated using the formula:

$$\text{Wound closure rate (\%)} = \frac{w(0) - w(t)}{w(0)} \times 100,$$

where $w(0)$ = wound area at time 0 and $w(t)$ is wound area at specific time.

Metabolite profiling

One dimensional ^{1}H-NMR analysis was performed on the hexane fraction according to procedure reported previously using a 500 MHz Varian INOVA NMR spectrometer (Varian Inc., Palo Alto, CA, USA). The sample was first dissolved in deuterated methanol (CD_3OD) and potassium dihydrogen phosphate (KH_2PO_4) buffer before sonication and centrifugation. Supernatant obtained was subjected to NMR analysis using a presaturation (PRESAT) setting mode. ^{1}H-NMR peak assignment was carried out by comparing the metabolite peaks with standard NMR databases and previous studies [19, 20], aided by Chenomx NMR software (Version 5.1, Alberta, Canada).

Molecular docking analysis

Molecular docking simulation of (1) isoschaftoside, (2) clinacoside C and (3) clinacoside B (Fig. S1) found in the leaves extract of *C. nutans* [15] was performed in the Nrf2 binding site of Keap 1 (PDB ID: 4L7B) [21] by using Schrödinger modeling software (Maestro version 12.7). The structures of ligands were prepared, optimized via LigPrep, and minimized under OPLS-2005 force field. Possible ionization states of the structure at neutral pH 7 were generated using Epik program. For each ligand, at most 8 tautomers and 32 stereoisomers per ligand were set to be generated. Crystal structure of Keap1 was obtained from the Protein Data Bank. The protein structure was first prepared using the Protein Preparation module in Maestro.

Docking grid was centered on the binding site of the co-crystallized ligand, IVV (inhibitor of Nrf2-Keap1 complex formation) according to coordinates of x: −3.37, y: 2.28, z: −27.55. The active site residues within the grid box consisted of Tyr334, Ser363, Asn414, Arg415, Ser508, Gln530, Ser555, Tyr572 and Ser602 [21–23]. The docking calculations were performed using Glide Extra Precision (XP) protocol [24–26]. Active site residues were kept rigid while flexible ligand sampling was used during the docking process. Post-docking minimization in the field of receptor was performed to produce better poses of ligand. Subsequently, binding orientations and interactions of each ligand with active site residues were analyzed. Binding orientation with the highest docking score was then selected for each ligand.

Statistical analysis

IBM SPSS version 21.0 was used to analyze the obtained experimental results. Data were initially tested for homogeneity of variances by the Levene test. For multiple comparison, one-way analysis of variance (ANOVA) was performed, followed by the Tukey test (when variances were found to be homogenous) or the Tamhane test (when variances were not homogenous). For comparison of just two sample groups, data were subjected to unpaired sample t-test. Every data was examined at the level of significance where $p < 0.05$. All *in vitro* experiments were performed in triplicates ($n = 3$).

RESULTS

Cytotoxic effect of *C. nutans* leaves fractions on HepG2 cell line

The 4 fractions (hexane, ethyl acetate, butanol, and water) of *C. nutans* leaves extract (CNL) were found non-toxic to HepG2 liver cells when evaluated at a wide concentration range of 5 µg/ml to 100 µg/ml (Fig. 1). Nevertheless, pro-proliferative effect was observed as cellular viability was enhanced as compared to the untreated control. Concentrations 6.25, 12.5, 25 µg/ml were selected for subsequent analyses.

Intracellular ROS level in HepG2 cell line treated with *C. nutans* leaves fractions before and after oxidative stress

The effects of the four CNL fractions (hexane, ethyl acetate, butanol, and water) towards the innate ROS levels were examined. It was found that all tested concentrations of hexane, ethyl acetate, n-butanol, and water fractions were able to maintain or decrease innate ROS as compared to untreated control cells. The positive control, tert-butyl hydroperoxide (t-BOOH) induced an exponential increased of ROS as expected. This was a strong indication that the cell model system established was working well (Fig. 2).

Protective effects of *C. nutans* fractions (hexane and ethyl acetate) towards oxidative stress induced HepG2 cells were determined. Based on Fig. 3, cells pre-treated with hexane, ethyl acetate, and n-butanol fractions of CNL were able to reduce ROS level by 25.32%, 19.31% and 14.86%, respectively, at concentration of 25 µg/ml, when measured at 60 min. However, ROS level in water fraction-treated cells was reduced by a mere 2% indicating that the protective effect was not prominent during oxidative stress. ROS reduction in hexane and ethyl acetate fractions-treated cells were further increased at 120 min. Nevertheless, the hexane treated group was observed to be most protected from oxidative stress compared to others based on its low ROS level.

The effect of *C. nutans* leaves fractions on reduced glutathione (GSH) level in HepG2 cells

The level of GSH per mg protein was assessed in HepG2 cells. Hexane and ethyl acetate fractions were selected for this assay as both fractions showed promising ROS reduction during oxidative stress. Based on the results, hexane and ethyl acetate at 25 µg/ml concentration increased GSH levels by 3-fold and 2.36-fold, respectively in liver cells as compared to untreated control (Fig. 4). Hexane again demonstrated superior activity as compared to the ethyl acetate fraction.

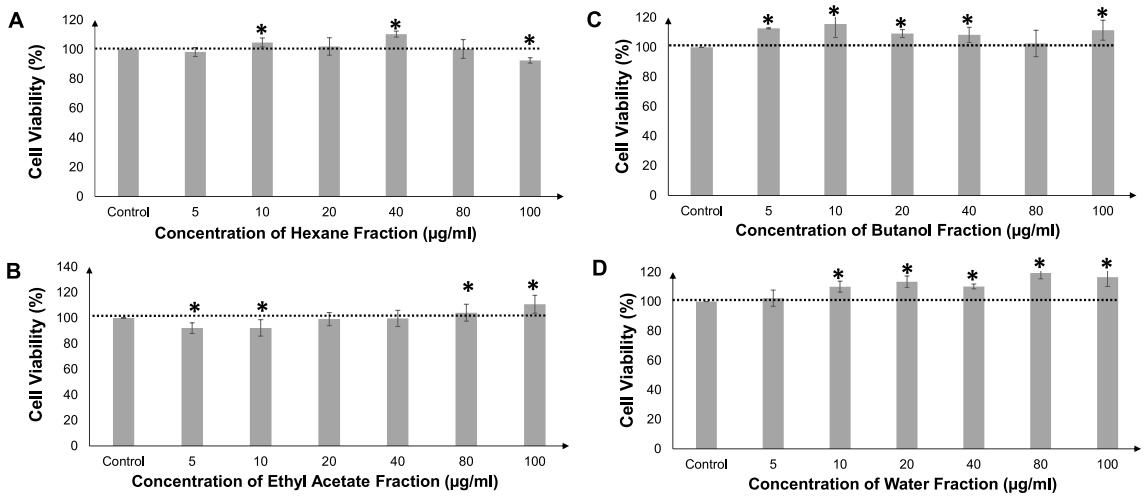

Fig. 1 HepG2 cell viability after pre-treatment with (A) hexane, (B) ethyl acetate, (C) n-butanol and (D) water fractions at concentrations ranging from 5 to 100 µg/ml. Experiments were performed in triplicates and expressed as means ± standard deviations. Data were analyzed by comparing viability of treated groups versus untreated control using unpaired sample *t*-test. Values with symbol *, are significantly different at $p < 0.05$.

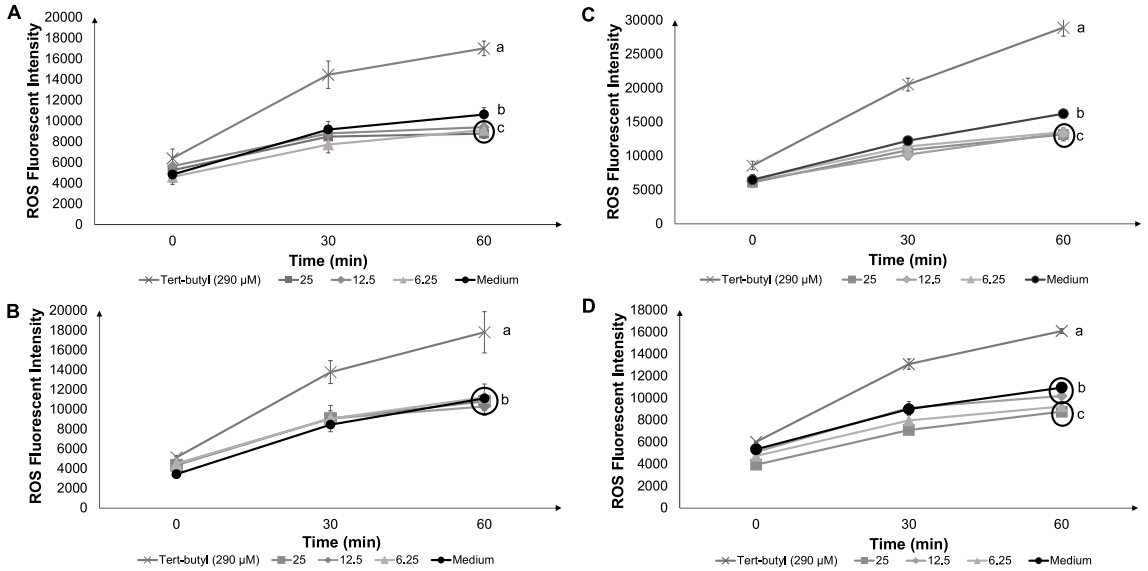

Fig. 2 Reduction of innate ROS level in HepG2 cells after treatment with (A) hexane, (B) ethyl acetate, (C) n-butanol and (D) water fractions at various concentrations. ROS production was observed for 60 min using the DCFH-DA assay. Experiments were performed in triplicates and expressed as means ± standard deviations. One-way ANOVA was used to compare the variances between different samples at 60 min. Means with different alphabets are significantly different at $p < 0.05$.

WJ-MSCs cytotoxicity effects, cell migration and proliferation after hexane and ethyl acetate treatments

The hexane and ethyl acetate fractions of CNL did not demonstrate cytotoxicity towards the WJ-MSCs even when the concentration was increased to 100 µg/ml (Fig. 5A). This result indicated that both fractions were likely safe for human use. The hexane and ethyl acetate fractions reduced the wound closure in a dose-dependent manner. The hexane fraction at the lowest concentration insignificantly enhanced the wound closure compared to the control group. As for the ethyl acetate fraction, the wound closure was significantly inhibited when the concentration increased to 50 µg/ml (Fig. 5B). No significant difference was found for the population doubling time (PDT) of hexane fraction compared to the control group. However, ethyl acetate

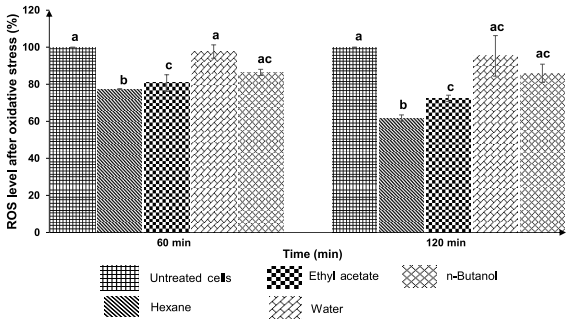

Fig. 3 ROS level in oxidative stress-induced HepG2 cells pre-treated with 25 µg/ml of hexane, ethyl acetate, water, and n-butanol fractions as compared to untreated control. Experiments were performed in triplicates and expressed as means ± standard deviations. One-way ANOVA was used to compare the variances between different samples at 60 min and 120 min, respectively. Means with different alphabets are significantly different at $p < 0.05$.

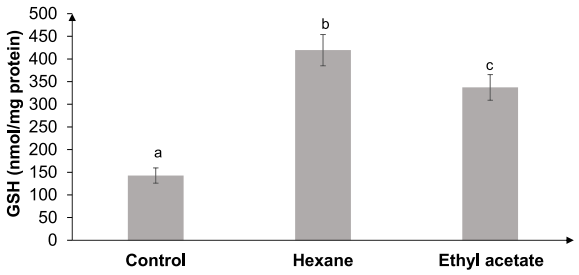

Fig. 4 The production of GSH per mg protein in HepG2 cells treated with hexane and ethyl acetate fractions. All values were performed in triplicates and expressed as means ± standard deviations ($n = 3$). One-way ANOVA was used to compare the variance between different samples. Means with different alphabets are significantly different at $p < 0.05$.

fraction has significantly longer PDT compared to the control group and the PDT was found to increase in a dose-dependent manner (Fig. 5C).

^{1}H-NMR spectra of hexane fraction and metabolite identification

Bioactive metabolites in CNL hexane fraction were identified using ^{1}H-NMR spectra as shown in Table S1. The phytocompounds detected included sulfur-containing glycosides (cycloclinacoside A1, cycloclinacoside A2, clinacoside A, clinacoside B and clinacoside C), flavones (schaftoside, isoschaftoside, and isovitexin), terpenoids (stigmasterol, and β-sitosterol), flavanols (catechin and epigallocatechin) and gallic acid. The three compounds postulated to be the active phytochemicals in our earlier study [15]; clinacoside C, clinacoside B and isoschaftoside were also found in the hexane fraction. Selected compounds were subjected to further computational analysis to identify their potentials as Nrf2 activators through molecular docking techniques.

Table 1 Docking scores of the compounds based on Glide XP docking protocol.

Compound	Docking score (kcal/mol)
Isoschaftoside	−12.609
Clinacoside C	−10.797
Clinacoside B	−9.496

Molecular docking of bioactive compounds derived from hexane fraction against Keap1

The co-crystallized ligand, IVV (a cysteine-independent activator of Nrf2) in the crystal structure of Keap1 (PDB ID: 4L7B) was re-docked into the binding pocket of Keap1 protein to validate the docking protocols used in the present study. The binding pose of the re-docked ligand was subsequently compared with that of the co-crystallized ligand; both ligands were found to superimpose well onto each other within the binding pocket of 4L7B (Fig. S2). The RMSD between the re-docked IVV and co-crystallised 4L7B was found to be 0.3678 Å. Based on the threshold value of 2.0 Å described by Gohlke et al [27] which differentiated the correct and incorrect docking solutions, it indicated that the docking protocols used in this study could well predict the binding poses and interactions of ligands in the binding site of 4L7B.

Based on the docking results, the phenol ring of (1) isoschaftoside was oriented into the central pore of binding pocket and the α-L-arabinopyranosyl moiety extended outwards (Fig. 6A). The ligand interacted with different binding site residues in proximity. Particularly, it formed hydrogen bonding with Tyr344, Arg415, Ser508 and Ser555; one of the hydroxyl groups on α-L-arabinopyranosyl moiety was hydrogen bonded to the hydroxyl side chain of Tyr344, while the other hydroxyl groups on β-D-glucosyl moiety were hydrogen bonded to the guanidinium side chain and hydroxyl side chains of Arg415 as well as Ser508 and Ser555, respectively. In addition, hydrophobic residues, such as Ile461, Tyr525, Ala556, Tyr572 and Phe577 bordered the non-polar moieties of the ligand. Polar residues including Ser363 and Gln530 were found to interact with adjacent carbonyl group of flavone moiety and hydroxyl groups of the ligand, respectively (Fig. 6A,B).

For (2) clinacoside C and (3) clinacoside B, the glucosyl moiety of the ligands faced inwards of the binding pocket while the sulfoxide moiety was directed outwards (Fig. S3A and Fig. S4A). Similarly, both ligands engaged in the same types of binding interactions with the residues in vicinity, such as hydrogen bonding and hydrophobic interactions. Clinacoside C was observed to form hydrogen bonding with nearby residues, namely Leu365, Ile416, Arg415, Val463, Gln530,

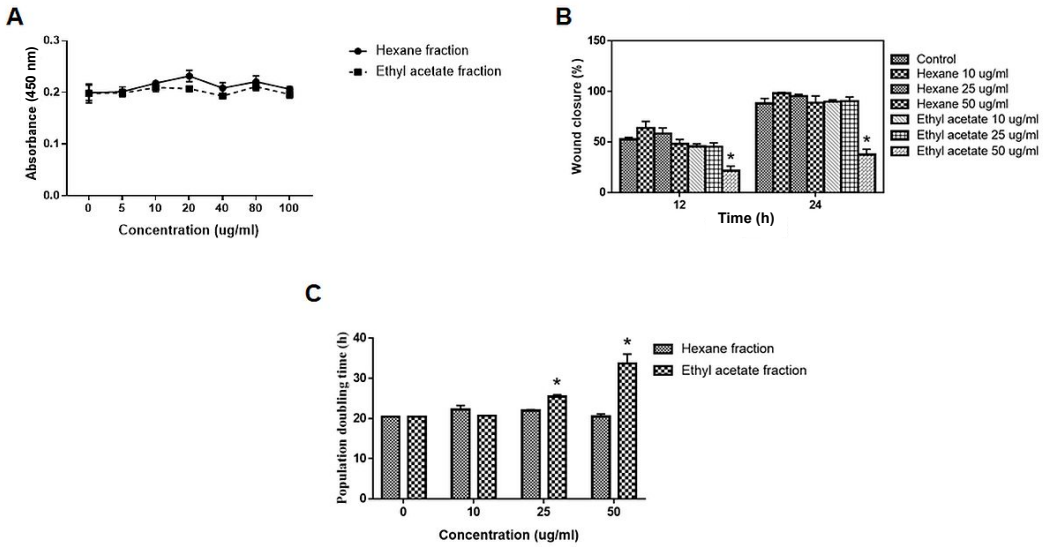

Fig. 5 Effect of hexane and ethyl acetate fractions on (A) cytotoxicity, (B) migration and (C) proliferation of WJ-MSCs. All values were performed in triplicates and expressed as means ± standard deviations ($n = 3$). Asterisks (*) represent $p < 0.05$ compared to the control group without extract.

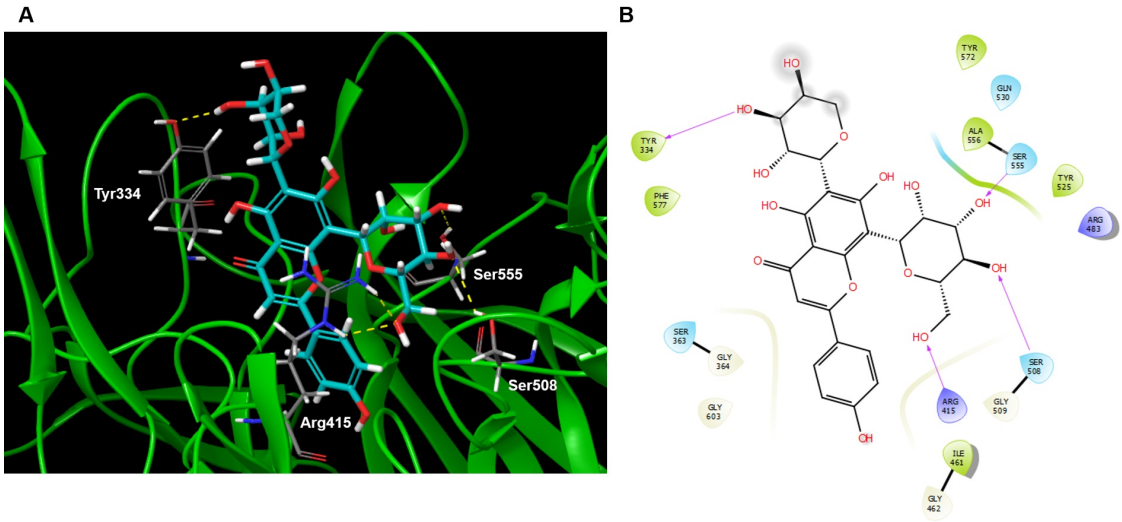

Fig. 6 (A) Binding orientation of isoschaftoside (highlighted in blue) in the binding pocket of Keap1 (PDB ID: 4L7B). Yellow dotted line: hydrogen bonding. (B) 2D ligand interaction diagrams of isoschaftoside illustrating interactions between the ligand and binding site residues. Purple line: hydrogen bonding. The docking was performed using Schrödinger modeling software (Maestro version 12.7).

Ser555 and Leu557. Hydroxyl groups on glucosyl moiety were hydrogen bonded to the backbone carbonyl groups of Leu365, Ile416, Val463 and Leu557. Hydrogen bondings were also formed between carbonyl group on the amide moiety and the guanidinium side chain of Arg415 as well as between sulfoxide moiety and the amido side chain and hydroxyl side chain of Gln530 and Ser555, respectively. The ligand was surrounded by hydrophobic residues as well, such as Ala366, Tyr525, Ala556 and Tyr572 via their alkyl group or aromatic ring side chain. Besides, the carbonyl group on amide moiety was also found to interact with adjacent polar residue, Ser508 (Fig. S3A,B). Clinacoside B was also engaged in hydrogen bonding with backbone carbonyl groups of Leu365, Ile416, Ala510 and Val604 as well as guanidinium side chain of Arg415 through the hydroxyl groups on its glucosyl moiety. Interactions with adjacent aromatic ring

Table 2 Binding interactions along with interacting moieties and residues identified for isoschaftoside, clinacoside C, and clinacoside B.

Compound	Binding interactions	Interacting moieties and residues
Isoschaftoside	Hydrogen bondings	Hydroxyl group on α-L-arabinopyranosyl moiety (Tyr344); hydroxyl groups on β-D-glucosyl moiety (Arg415, Ser508, Ser555)
	Hydrophobic interactions	Non-polar moieties (Ile461, Tyr525, Ala556, Tyr572, Phe577)
	Other polar interactions	Carbonyl group of flavone moiety (Ser363); hydroxyl groups (Gln530)
Clinacoside C	Hydrogen bondings	Hydroxyl groups on glucosyl moiety (Leu365, Ile416, Val463, Leu557); carbonyl group on the amide moiety (Arg415); sulfoxide moiety (Gln530, Ser555)
	Hydrophobic interactions	Non-polar moieties (Ala366, Tyr525, Ala556, Tyr572)
	Other polar interactions	Carbonyl group on amide moiety (Ser508)
Clinacoside B	Hydrogen bondings	Hydroxyl groups on its glucosyl moiety (Leu365, Ile416, Ala510, Val604, Arg415)
	Hydrophobic interactions	Non-polar moieties (Tyr525, Ala556)
	Other polar interactions	Sulfoxide moiety (Ser508, Ser555)

and alkyl side chains of hydrophobic residues, namely Tyr525 and Ala556 as well as with polar residues, such as Ser508 and Ser555 through its sulfoxide moiety were also observed with such ligand (Fig. S4A,B). Superimposition of the three ligands in the binding cleft is illustrated in Fig. S5 of SD. The docking scores of the compounds are tabulated in Table 1. Additionally, the binding interactions and interacting moieties and residues identified for isoschaftoside, clinacoside C and clinacoside B are summarized in Table 2.

DISCUSSION

Methanolic leaves extract of *C. nutans* (Burm.f.) Lindau demonstrated good antioxidative activities in our earlier work [15]. Based on the multivariate analysis, we postulated that the three major phytocompounds; clinacoside B, clinacoside C and isoschaftoside, contributed to the bioactivities. In this study, we identified the most active *C. nutans* leaves fractions and the metabolites responsible for both the antioxidant and regenerative potentials. Outcomes from this work could validate the results obtained from our previous experiments [15].

In order to advance to cell-based antioxidant assays, the cytotoxicity of each 4 fractions of CNL (hexane, ethyl acetate, n-butanol, and water) at concentration range of 5 µg/ml to 100 µg/ml were assessed using HepG2 liver cell line. It was found that all fractions were not cytotoxic at concentration of 100 µg/ml and below. This was supported by Md Toha et al [28], who reported that *C. nutans* hexane and water fractions did not display significant inhibitory effects towards human breast cancer cell line (MCF-7) within the concentration range of 31.25 µg/ml to 500 µg/ml. In another study, hexane and ethyl acetate fractions of *C. nutans* even at a high dose of 400 µg/ml did not exhibit toxicity towards the normal colon cell line (CCD-18Co) [29]. Hence, the tested concentrations were deemed to be safe for use in subsequent cell-based assays.

The effects of CNL fractions on cellular ROS reduction were determined using DCFH-DA assay on HepG2 cell line. In normal condition, the level of ROS is well regulated by endogenous antioxidants to achieve cellular physiological homeostasis. Sometimes exogenous antioxidants are required to facilitate cellular redox balance. The major generator of cellular ROS is the mitochondrial oxidative metabolism that produces ROS as its biochemical byproduct [30]. The hexane, n-butanol, and water fractions of CNL were able to reduce innate ROS level significantly when compared to the untreated control (Fig. 2), whereas ethyl acetate maintained ROS at the basal level. The highest concentration of 25 µg/ml was selected and used for the determination of protective effects of CNL fractions towards induced-oxidative stress as it reduced ROS from basal level consistently as compared to other tested concentrations.

Overproduction of intracellular ROS during oxidative stress can damage the nucleic acids as well as modify the structure and function of cellular lipids and proteins, eventually leading to the induction of cell death through apoptosis or necrosis [31]. Based on Fig. 3, hexane was a superior antioxidant as it produced the highest ROS reduction in liver cells during tert-butyl hydroperoxide induced oxidative stress,

followed by ethyl acetate and the other fractions. One of the mechanisms to counteract oxidative stress is to elevate the intracellular antioxidant levels, mainly the GSH [4]. Hence, the two best fractions (hexane and ethyl acetate) were further assessed for their GSH enhancing properties.

GSH is one of the major nonenzymatic antioxidant defenses in the cell. This molecule acts as a co-factor in glutathione peroxidase-catalyzed detoxification of organic peroxides. It also neutralizes free radicals through electron-transfer reaction and participates in metal chelating activities [32]. Intriguingly, both the tested fractions significantly increased GSH contents in liver cells as compared to untreated control by 2- to 3-fold higher (Fig. 4). The hexane fraction contributed to a higher cellular GSH level than the ethyl acetate fraction which was in line with the results from the ROS assay indicating hexane as a stronger antioxidant. Similar GSH-enhancing results were reported by other plant extracts. For example, seed extract of *Ammi visnaga* (L.) Lam. was found to elevate GSH content in human liver cancer cell line (HuH-7 cells) significantly at 500 µg/ml and 1000 µg/ml [33]. In another study, *Clerodendrum cyrthophyllum* Turcz. leaves extract also increased the intracellular glutathione of HepG2 cells by 13.8% in comparison to untreated control [34]. GSH levels could be enhanced intracellularly mainly through the activation of Nrf2. This is because Nrf2 is a redox-sensitive transcription factor which regulates glutathione level and maintains the reduced/oxidized GSH/GSSG ratio [4]. We also investigated via *in silico* method the inhibition of Keap1 (the inhibitor of Nrf2) by selected phytocompound in this study as well.

The regenerative potentials of hexane and ethyl acetate fractions were determined towards WJ-MSCs. Both fractions were not cytotoxic to the stem cells even at the highest concentration of 100 µg/ml similar to the toxicity test performed on HepG2 cell line (Fig. 5A). Thus, these fractions were considered safe for human use. Further analysis on cell proliferation and migration assays found that both fractions were unable to significantly enhance stem cell proliferation and migration. In fact, the ethyl fraction at high concentrations retarded cell proliferation and migration. The hexane fraction appeared to possess better regenerative potential compared to the ethyl acetate fractions as it could maintain the stem cell proliferation and migration even at the highest concentration of 50 µg/ml (Fig. 5B,C).

Since hexane fraction of CNL was more promising than ethyl acetate fraction based on antioxidative and regenerative activities, its secondary metabolites profile was obtained through ^{1}H-NMR. Phytocompounds detected in this fraction included sulfur-containing glucosides, flavones, terpenoids and flavanols. Based on Table S1, the hexane fraction also contained all three compounds (clinacoside B, clinacoside C, and isoschaftoside) that were postulated in our earlier work to be responsible for the antioxidant nature of *C. nutans* leaves extract. Therefore, clinacoside B, clinacoside C, and isoschaftoside were further used for molecular docking analysis to determine their potential as a Nrf2 activator.

Direct inhibition of the Keap1-Nrf2 protein-protein interaction has been regarded as an alternative strategy to tackle oxidative stress implicated in various diseases [35]. Studies had reported that compounds that could interact with Keap1 and occupy Nrf2 binding site in the protein could eventually induce transcriptional activation of Nrf2, leading to expression of ARE-dependent genes and other antioxidative enzymes which included GSH [16, 36, 37]. In the present molecular docking studies, binding orientation and interactions of isoschaftoside (1), clinacoside C (2), and clinacoside B (3) in the Nrf2 binding site of Keap1 protein were investigated. Isoschaftoside was observed to make interaction with adjacent residues in different subpockets (P1–P5) of Keap1 [22] mainly through hydrogen bonding and hydrophobic interactions (Fig. 6A,B). Amongst these residues, Tyr334, Ser363, Arg415, Ser508, Gln530, Ser555 and Tyr572 had been reported as the key residues in the structure of Keap1-Nrf2 interface [21–23]. On the other hand, clinacoside C (Fig. S3A,B) and clinacoside B (Fig. S4A,B) were found to interact with residues in the P1, P3 and P4 subpockets of Keap1 protein mostly via hydrogen bonding and hydrophobic interaction as well. Both ligands were able to engage with several important binding site residues, for instances Arg415, Ser508, Gln530, Ser555 and Tyr572. Of note, the glucosyl and pyranosyl moieties in these three compounds had indeed contributed considerable interactions with the binding site residues, particularly via hydrogen bonding. This finding suggested that the presence of hydrogen bond acceptors or donors in the ligand was important to establish binding interactions in the binding pocket of Keap1. This is consistent with the results by Li and co-workers [37] which reported that compounds with abundant oxygen or sugar moieties could inhibit the Keap1-Nrf2 interaction more effectively. Besides, docking scores of the ligands were also examined (Table 1); the score is derived from the scoring function evaluating the binding pose and interaction of a ligand inside the binding pocket of a target protein [24–26]. Ligands with more negative values are indicated as tighter binders. Isoschaftoside demonstrated the highest negative docking score (−12.609 kcal/mol) among the three compounds, inferring that its binding affinity in the binding pocket of Keap1 was higher than that of clinacoside C and clinacoside B. The higher binding affinity and engagement with many key amino acids of Keap1-Nrf2 interface as observed with isoschaftoside implied that such compound warrants further investigation for its potential

as inhibitor of Keap1-Nrf2 complex formation to subsequently activate the Nrf2 leading to transcription of ARE-dependent genes and antioxidative enzymes.

Recently, a xanthone, demethylcalabaxanthone, isolated from *Garcinia mangostana* was reported to directly inhibit Keap1 via interaction with amino acids belonging to the five subpockets. This compound formed non-covalent bonding with key amino acid residues similar to isoschaftoside. Furthermore, it was found to enhance GSH levels in SH-SY5Y neuroblastoma cells during induced oxidative stress which could be due to Nrf2 activation after Keap1 inhibition [38]. Flavonoids such as naringenin, hesperetin, and narirutin, exhibited strong Keap1 inhibitory effects as well. These citrus-derived flavonoids demonstrated promising ARE activation activity in HEK293T embryonic kidney cells [39]. Ten small peptides derived from *Chinemys reevesii* or better known as Chinese pond turtle, demonstrated competitive inhibitory action towards Keap1 active site, thus, activating the Nrf2/Keap1 signaling in *Drosophila melanogaster*. Interaction of these peptides with important amino acid residues of Keap1 was revealed to be the same as isoschaftoside [40].

Isoschaftoside was mentioned to reverse NAFLD through activation of autophagy [41]. In view of that, results from this study corroborated well with the previous work performed. The mode of action of this C-glycosyl flavonoid may not be via just a single pathway but could be regulating multiple pathways simultaneously to alleviate NAFLD. Our study clearly indicated isoschaftoside as a possible Nrf2 activator that could boost the antioxidative capacity of liver cells, thus, overcoming the progression of this liver disease.

CONCLUSION

The hexane fraction of *C. nutans* leaves extract displayed promising liver protective potential *in vitro* as compared to other tested fractions. Isoschaftoside present in this fraction could be a promising molecule contributing to the observed bioactivities since it was shown to inhibit Keap1 *in silico*. This phenomenon could indirectly activate Nrf2, a prominent key player in cellular antioxidative effect. Nevertheless, more in depth investigation on the interaction between isoschaftoside and Keap1 should be conducted to validate the computational work and to support its usage for NAFLD.

Appendix A. Supplementary data

Supplementary data associated with this article can be found at https://dx.doi.org/10.2306/scienceasia1513-1874.2025.039.

Acknowledgements: This work was financially supported by Tunku Abdul Rahman University of Management and Technology (TARUMT) through the TAR UC Internal Research Grant Scheme, project number: UC/I/G2017-00021.

REFERENCES

1. Li B, Zhang C, Zhan YT (2018) Nonalcoholic fatty liver disease cirrhosis: A review of its epidemiology, risk factors, clinical presentation, diagnosis, management, and prognosis. *Can J Gastroenterol Hepatol* **2018**, 3541365.
2. Qi WW, Liu Y, Liu PF, Yi M, Zhang C, Zhang S, Zhong LY (2024) 11β-hydroxysteroid dehydrogenase type 1 selective inhibitor alleviates insulin resistance and non-alcoholic fatty liver disease in db/db mice. *ScienceAsia* **50**, 2024076.
3. Khan A, Ross HM, Parra NS, Chen SL, Chauhan K, Wang M, Yan B, Magagna J, et al (2022) Risk prevention and health promotion for non-alcoholic fatty liver diseases (NAFLD). *Livers* **2**, 264–282.
4. Arroyave-Ospina JC, Wu Z, Geng Y, Moshage H (2021) Role of oxidative stress in the pathogenesis of non-alcoholic fatty liver disease: Implications for prevention and therapy. *Antioxid* **10**, 174.
5. García-Ruiz C, Fernández-Checa JC (2018) Mitochondrial oxidative stress and antioxidants balance in fatty liver disease. *Hepatol Commun* **2**, 1425–1439.
6. Zhang C, Wang N, Xu Y, Tan HY, Li S, Feng Y (2018) Molecular mechanisms involved in oxidative stress-associated liver injury induced by Chinese herbal medicine: An experimental evidence-based literature review and network pharmacology study. *Int J Mol Sci* **19**, 2745.
7. Conde de la Rosa L, Goicoechea L, Torres S, Garcia-Ruiz C, Fernandez-Checa JC (2022) Role of oxidative stress in liver disorders. *Livers* **2**, 283–314.
8. Delli Bovi AP, Marciano F, Mandato C, Siano MA, Savoia M, Vajro P (2021) Oxidative stress in non-alcoholic fatty liver disease. An updated mini review. *Front Med* **8**, 1–14.
9. Mantovani A, Dalbeni A (2021) Treatments for NAFLD: State of art. *Int J Mol Sci* **22**, 2350.
10. Chen Q, Wang T, Li J, Wang S, Qiu F, Yu H, Zhang Y, Wang T (2017) Effects of natural products on fructose-induced non-alcoholic fatty liver disease (NAFLD). *Nutrients* **9**, 96.
11. Ong WY, Herr DR, Sun GY, Lin TN (2022) Anti-inflammatory effects of phytochemical components of *Clinacanthus nutans*. *Molecules* **27**, 3607.
12. Chia TY, Gan CY, Murugaiyah V, Hashmi SF, Fatima T, Ibrahim L, Abdulla MH, Alswailmi FK, et al (2021) A narrative review on the phytochemistry, pharmacology and therapeutic potentials of *Clinacanthus nutans* (Burm. f.) lindau leaves as an alternative source of future medicine. *Molecules* **27**, 139.
13. Teoh PL (2020) A minireview on phytochemical and medicinal properties of *Clinacanthus nutans*. *J Appl Pharm Sci* **11**, 15–21.
14. Wongmaneeroj M, Jamjumrus S, Agarum R, Sukkhaeng S, Promdang S, Homhual R (2023) Effects of growth regulators on production of bioactive compounds from *Clinacanthus nutans* (Burm.f.) Lindau Phaya Yo culture *in vitro*. *ScienceAsia* **49**, 864–872.
15. Ng KS, Tan SA, Bok CY, Loh KE, Ismail IS, Yue CS, Loke CF (2022) Metabolomic approach for rapid identification of antioxidants in *Clinacanthus nutans* leaves with liver protective potential. *Molecules* **27**, 3650.
16. Tan SA, Goya L, Ramanathan S, Sulaiman SF, Alam M, Navaratnam V (2014) Chemopreventive effects of standardized papaya leaf fraction on oxidatively stressed

human liver cells. *Food Res Int* **64**, 387–395.
17. Slamenova D, Kozics K, Hunakova L, Melusova M, Navarova J, Horvathova E (2013) Comparison of biological processes induced in HepG2 cells by tert-butyl hydroperoxide (t-BHP) and hydroperoxide (H_2O_2): The influence of carvacrol. *Mutat Res* **757**, 15–22.
18. Tsai TH, Yu CH, Chang YP, Lin YT, Huang CJ, Kuo YH, Tsai PJ (2017) Protective effect of caffeic acid derivatives on tert-butyl hydroperoxide-induced oxidative hepatotoxicity and mitochondrial dysfunction in HepG2 cells. *Molecules* **22**, 702.
19. Khoo LW, Kow AS, Maulidiani M, Ang MY, Chew WY, Lee MT, Tan CP, Shaari K, et al (2018) ^{1}H-NMR metabolomics for evaluating the protective effect of *Clinacanthus nutans* (burm. f) lindau water extract against nitric oxide production in LPS-IFN-γ activated raw 264.7 macrophages. *Phytochem Anal* **30**, 46–61.
20. Khoo LW, Mediani A, Zolkeflee NK, Leong SW, Ismail IS, Khatib A, Shaari K, Abas F (2015) Phytochemical diversity of *Clinacanthus nutans* extracts and their bioactivity correlations elucidated by NMR based metabolomics. *Phytochem Lett* **14**, 123–133.
21. Jnoff E, Albrecht C, Barker JJ, Barker O, Beaumont E, Bromidge S, Brookfield F, Brooks M, et al (2014) Binding mode and structure-activity relationships around direct inhibitors of the Nrf2-Keap1 Complex. *Chem Med Chem* **9**, 699–705.
22. Crisman E, Duarte P, Dauden E, Cuadrado A, Rodríguez-Franco MI, López MG, León R (2022) Keap1-Nrf2 protein-protein interaction inhibitors: Design, pharmacological properties and therapeutic potential. *Med Res Rev* **43**, 237–287.
23. Lo SC, Li X, Henzl MT, Beamer LJ, Hannink M (2006) Structure of the Keap1:Nrf2 interface provides mechanistic insight into Nrf2 signaling. *EMBO J* **25**, 3605–3617.
24. Friesner RA, Banks JL, Murphy RB, Halgren TA, Klicic JJ, Mainz DT, Repasky MP, Knoll EH, et al (2004) Glide: A new approach for rapid, accurate docking and scoring. 1. Method and assessment of docking accuracy. *J Med Chem* **47**, 1739–1749.
25. Friesner RA, Murphy RB, Repasky MP, Frye LL, Greenwood JR, Halgren TA, Sanschagrin PC, Mainz DT (2006) Extra precision glide: Docking and scoring incorporating a model of hydrophobic enclosure for protein-ligand complexes. *J Med Chem* **49**, 6177–6196.
26. Halgren TA, Murphy RB, Friesner RA, Beard HS, Frye LL, Pollard WT, Banks JL (2004) Glide: A new approach for rapid, accurate docking and scoring. 2. Enrichment factors in database screening. *J Med Chem* **47**, 1750–1759.
27. Gohlke H, Hendlich M, Klebe G (2000) Knowledge-based scoring function to predict protein-ligand interactions. *J Mol Biol* **295**, 337–356.
28. Md Toha Z, Haron NH, Kamal NN, Khairuddean M, Arsad H (2022) Exploring *Clinacanthus nutans* leaf different solvent extracts on antiproliferative effects induced metastasis through apoptosis and cell cycle against MCF-7 human breast cancer cell lines. *Future J Pharm Sci* **8**, 49.
29. Esmailli K, Shafaei A, Abdalrahim A, Alsuede F, Majid A, Ismail Z (2019) Evaluation of *in vitro* cytotoxicity effect of *Clinacanthus nutans* (Brum. f.) Lindau standardized leaf extracts. *Trop J Pharm Res* **18**, 2341–2348.
30. Zhang J, Wang X, Vikash V, Ye Q, Wu D, Liu Y, Dong W (2016) ROS and ROS-mediated cellular signalling. *Oxid Med Cell Longev* **2016**, 4350965.
31. Kim S, Kim M, Kang MC, Lee HH, Cho CH, Choi I, Park Y, Lee SH (2021) Antioxidant effects of turmeric leaf extract against hydrogen peroxide-induced oxidative stress *in vitro* in Vero cells and *in vivo* in zebrafish. *Antioxidants* **10**, 112.
32. Labarrere CA, Kassab GS (2022) Glutathione: A Samsonian life-sustaining small molecule that protects against oxidative stress, ageing and damaging inflammation. *Front Nutr* **9**, 1007816.
33. Arafah MW, Almutairi B, Al-Zharani M, Alkahtane AA, Al-Otibi FO, Ali D, Alghamdi WM, Alanazi IS, et al (2021) The protective effect of *Ammi visnaga* extracts against human hepatic cancer. *J King Saud Univ Sci* **33**, 101540.
34. Zhu J, Li G, Zhou J, Xu Z, Xu J (2022) Cytoprotective effects and antioxidant activities of acteoside and various extracts of *Clerodendrum Cyrtophyllum* Turcz leaves against t-BHP induced oxidative damage. *Sci Rep* **12**, 12630.
35. Magesh S, Chen Y, Hu L (2012) Small molecule modulators of Keap1-Nrf2-ARE pathway as potential preventive and therapeutic agents. *Med Res Rev* **32**, 687–726.
36. Pang C, Zheng Z, Shi L, Sheng Y, Wei H, Wang Z, Ji L (2016) Caffeic acid prevents acetaminophen-induced liver injury by activating the Keap1-Nrf2 antioxidative defense system. *Free Radic Biol Med* **91**, 236–246.
37. Li M, Huang W, Jie F, Wang M, Zhong Y, Chen Q, Lu B (2019) Discovery of Keap1-Nrf2 small-molecule inhibitors from phytochemicals based on molecular docking. *Food Chem Toxicol* **133**, 110758.
38. De Vita S, Masullo M, Grambone S, Bescós PB, Piacente S, Bifulco G (2023) Demethylcalabaxanthone from *Garcinia mangostana* exerts antioxidant effects through the activation of the Nrf2 pathway as assessed via molecular docking and biological evaluation. *Antioxidants* **12**, 1980.
39. Guan T, Bian C, Ma Z (2023) *In vitro* and *in silico* perspectives on the activation of antioxidant responsive element by citrus-derived flavonoids. *Front Nutr* **10**, 1257172.
40. Wang Q, Yang Z, Zhuang J, Zhang J, Shen F, Yu P, Zhong H, Feng F (2022) Antiaging function of Chinese pond turtle (*Chinemys reevesii*) peptide through activation of the Nrf2/Keap1 signaling pathway and its structure-activity relationship. *Front Nutr* **9**, 961922.
41. Su Y, Kang Y, Yi J, Lin Q, Zhang C, Lin Z, Yan Z, Qu J, et al (2022) Isoschaftoside reverses nonalcoholic fatty liver disease via activating autophagy *in vivo* and *in vitro*. *Evid Based Complementary Altern Med* **2022**, 2122563.

Appendix A. Supplementary data

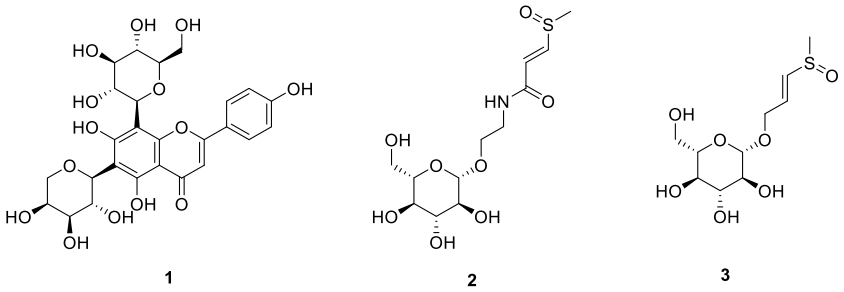

Fig. S1 (1) Isoschaftoside, (2) clinacoside C, and (3) clinacoside B present in the leaves extract of *C. nutans*.

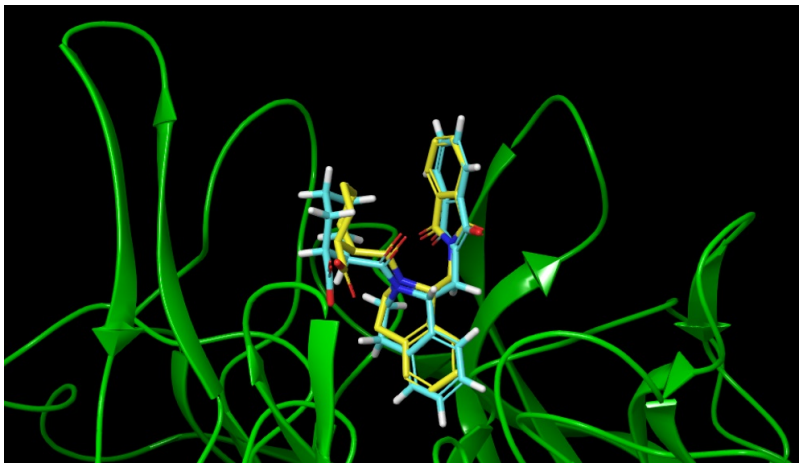

Fig. S2 Superimposition of re-docked IVV (cyan) with co-crystallized IVV (yellow) in the binding pocket of Keap1 (PDB ID: 4L7B).

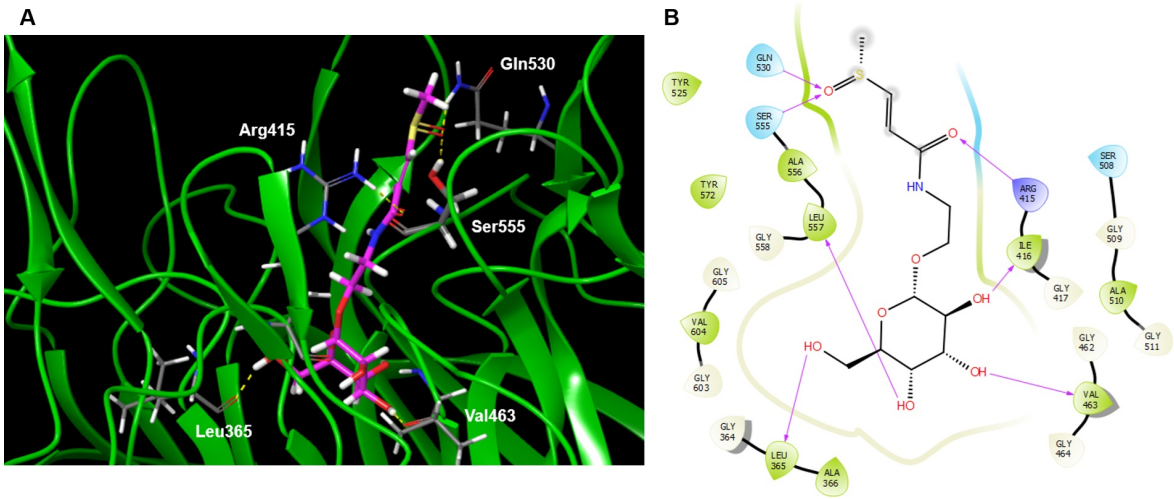

Fig. S3 (A) Binding orientation of clinacoside C (highlighted in magenta) in the binding pocket of Keap1 (PDB ID: 4L7B). Yellow dotted line: hydrogen bonding; hydrogen bonding with Ile416 and Leu557 were not shown. (B) 2D ligand interaction diagrams of clinacoside C illustrating interactions between the ligand and binding site residues. Purple line: hydrogen bonding.

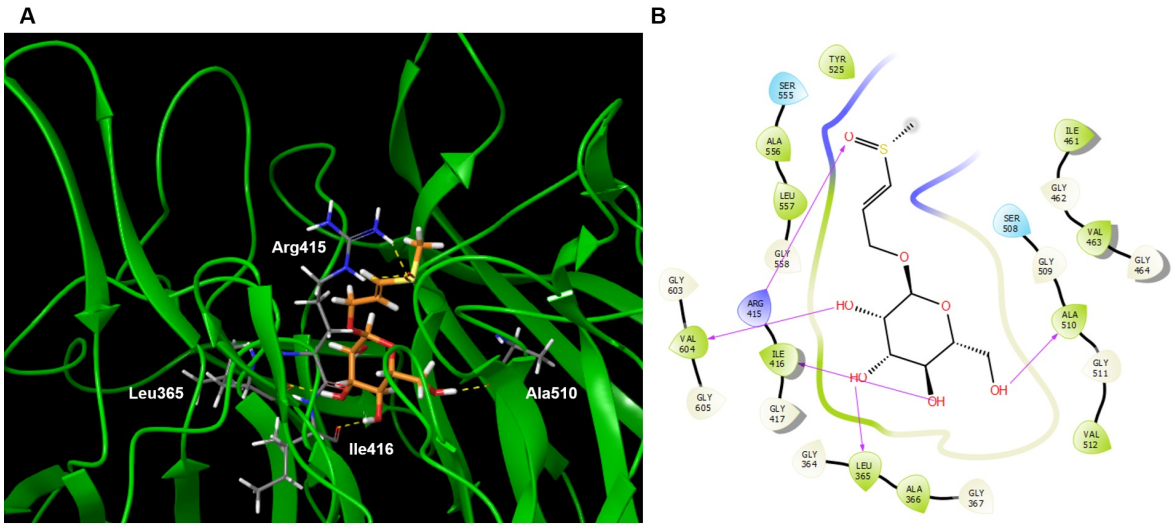

Fig. S4 (A) Binding orientation of clinacoside B (highlighted in orange) in the binding pocket of Keap1 (PDB ID: 4L7B). Yellow dotted line: hydrogen bonding; hydrogen bonding with Val604 was not shown. (B) 2D ligand interaction diagrams of clinacoside B illustrating interactions between the ligand and binding site residues. Purple line: hydrogen bonding.

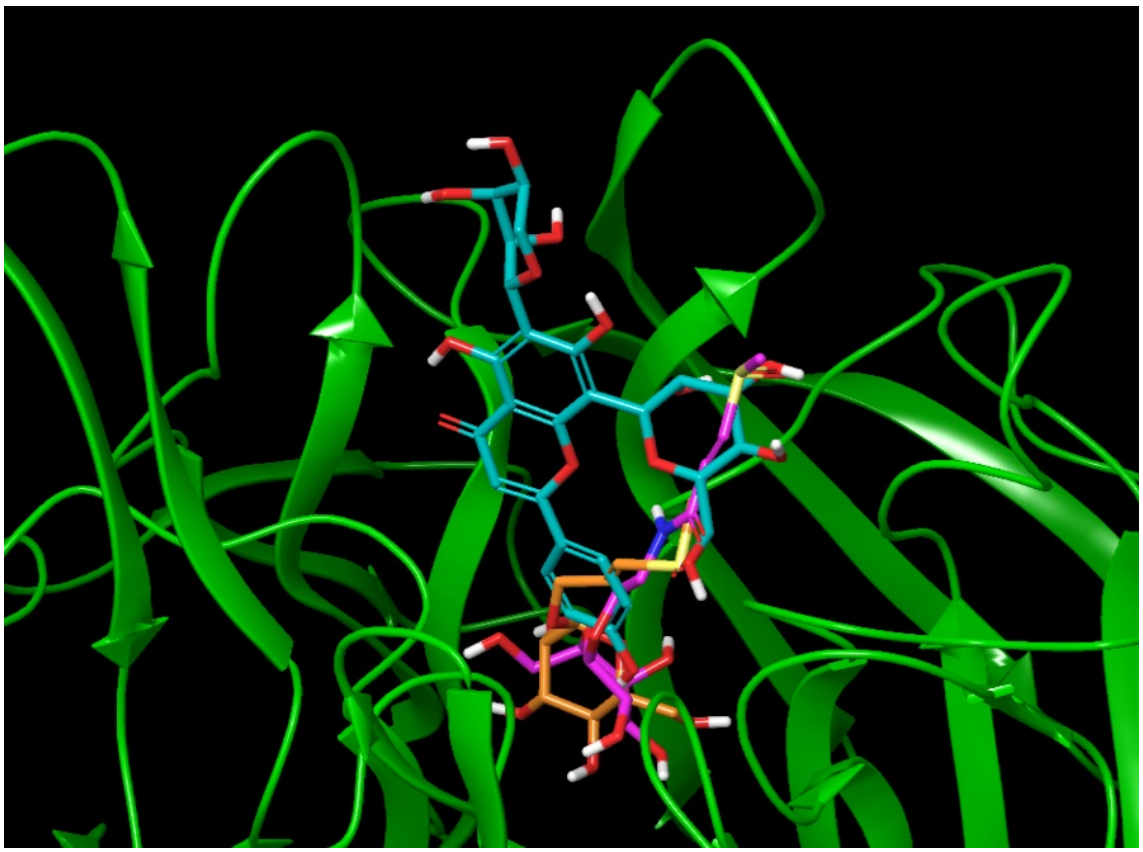

Fig. S5 Superimposition of isoschaftoside (blue), clinacoside C (magenta) and clinacoside B (orange) within the binding cleft of Keap1.

Table S1 Characteristic signals of metabolites identified in *C. nutans* hexane fraction based on ^{1}H-NMR spectra.

Metabolite	**^{1}H-NMR characteristic signals**
Secondary metabolite	
(1) Stigmasterol[a]	5.36 (m), 1.01 (s), 0.94 (d, J = 7 Hz), 0.79 (d, J = 1.9 Hz), 0.82 (d, J = 8.9 Hz), 0.94 (m)
(2) β-Sitosterol[a]	5.38 (d, J = 3.8 Hz), 1.01 (s), 0.94 (m), 0.79 (d, J = 1.9 Hz), 0.82 (d, J = 8.9 Hz)
(3) Clinacoside A[a]	4.7 (m), 4.12 (m), 4.1 (m), 3.81 (m), 2.9 (s)
(4) Clinacoside B[a]	6.94 (m), 4.01 (d, J = 9.6 Hz), 3.92 (m)
(5) Clinacoside C[a]	4.06 (m), 3.82 (m), 3.73 (m), 2.65 (s)
(6) Cycloclinacoside A1[a]	3.49 (m), 4.10 (m), 4.69 (m)
(7) Cycloclinacoside A2[a]	4.69 (m), 3.35 (s)
(8) Clinamide A[a]	6.94 (m), 3.66 (m), 3.47 (m), 3.09 (s)
(9) Clinamide B[a]	6.67 (d, J = 4.1 Hz), 4.17 (m), 3.54 (m), 2.76 (s), 2.06 (m)
(10) Isovitexin[a]	6.94 (m)
(11) Schaftoside[a]	8 (d, J = 8 Hz), 6.94 (m), 3.95–3.21 (m)
(12) Isoschaftoside[a]	8 (d, J = 8 Hz), 6.94 (m), 6.65 (d, J = 4.1 Hz), 4.07 (m), 4.01 (m), 3.85 (m), 3.75 (m), 3.64 (m), 3.53 (m), 3.47 (m)
(13) Epigallocatechin[a]	6.52 (s), 2.70 (d, J = 2.4 Hz)
(14) Catechin[a]	4.59 (m), 4.01 (m), 2.79 (m)
(15) Gallic acid[a]	6.94 (m)

Compounds with symbols ‘a’ represent identification that were previously reported in *C. nutans* by Khoo et al [19].